



Adsorption of lead ions on magnetically separable Fe₃O₄ watermelon composite

Kayode Adebowale¹ · Abisola Egbedina¹ · Blessed Shonde¹

Received: 3 July 2020 / Accepted: 8 September 2020 / Published online: 26 September 2020
© The Author(s) 2020

Abstract

The search for green methods for the synthesis of eco-friendly and sustainable materials is the focus of many studies. In this paper, magnetite nanoparticles (WM-Fe₃O₄) were synthesized using watermelon rind as a stabilizing agent and their adsorption capacity for the removal of lead ions was evaluated. The synthesized WM-Fe₃O₄ was characterized using Fourier transform infrared spectroscopy, X-ray diffraction and scanning electron microscopy. Adsorption capacity and mechanism of WM-Fe₃O₄ for the removal of lead ions from water were evaluated. The adsorption isotherms data were well described by both Langmuir and Freundlich isotherms showing the heterogeneous nature of the adsorbent. Adsorption kinetics followed the pseudo-second-order model which confirmed the heterogeneity of the adsorbent and shows that adsorption followed chemisorption. Adsorption capacity was found to be 138 mg/g for lead. The initial solution pH had an influence on the adsorption. The removal efficiency decreased after pH 7. Effect of varying adsorbent mass indicates that a low dosage is required thereby favouring industrial scale up. The adsorption of lead ions was mainly controlled by electrostatic attraction and polar interactions. This adsorbent has potentials for the efficient capture of heavy metals with possibilities for the future replacement of expensive adsorbents.

Keywords Green synthesis · Magnetite · Watermelon rind · Adsorption · Sustainable · Nanoparticles

Introduction

Heavy metal pollution is still a critical challenge in the field of environmental science. In a recent report, they have been classified as belonging to a group of contaminants referred to as emerging contaminants (Lodeiro et al. 2019). They are not biodegradable; generally immutable and therefore are persistent in the environment. They have the tendency to bioaccumulate into tissues of living organisms where they result in toxic effects (Abdus-Salam and Adekola 2018). Increasing industrialization has led to increase in the amounts of these pollutants entering into the environment from activities such as those of the textile, mining, cosmetic, pharmaceutical industries.

The search for economically feasible and environmentally sustainable methods for their removal from the environment has resulted in adsorption being the removal technique of

choice. Adsorption is a low-cost, highly efficient technology that does not result in the production of by-products that are even more toxic than the parent compounds. It is easy to operate, versatile and can be easily incorporated into current wastewater treatment technologies. Current researches are now geared towards the engineering of alternative hybrid adsorbents to the expensive activated carbon, and which have high pollutant binding capacities, low-cost with potentials for large scale treatment of wastewater (Pooi and Ng 2018), high stability and ease of operation (Abdus-Salam and Adekola 2018).

Magnetite nanoparticles have gained prominence in water treatment not only due to their ease of separation from aqueous solution but also due to their effectiveness as a result of their large surface area and economic viability. They also do not degrade and can be utilized for extended periods on a large scale. Several reports deal with the use of magnetite nanoparticles in wastewater treatment (Fisli et al. 2014; Lasheen et al. 2016; Adegoke et al. 2014). However, it presents the problem of bleeding and instability which results in agglomeration (Lasheen et al. 2016). This has prompted research into composites of magnetite that overcome the

✉ Abisola Egbedina
adeyemoabisola@yahoo.com

¹ Department of Chemistry, Faculty of Science, University of Ibadan, Ibadan, Oyo State, Nigeria

challenges listed above while retaining the special property of magnetism in the new material. This can be possible due to their ability to react with a variety of functional groups. Biomass materials are known to be polyfunctional and therefore are an excellent choice for a composite with magnetite. Watermelon is a highly consumed fruit in the world and Nigeria ranks among the twenty leading producers in the world (Toluwalase and Owoeye 2017). The watermelon rind takes up about 30% of the total mass of the fruit (Hind 2017) making it a useful abundant waste material.

This study describes the synthesis of a low-cost modified variation of magnetite from watermelon rind biomass (WM-Fe₃O₄). This results in a waste-to-wealth approach in the synthesis of an environmentally sustainable material. Moreover, this material prepared also does not make use of chemicals which can further pose threats to the environment.

Experimental section

Materials

Watermelon rinds were gathered from a local market in Ibadan, Nigeria. Afterwards, they were washed thoroughly, sun-dried for 72 h and transferred to an oven for 48 h at 105 °C. This was followed by grinding in a mill to obtain fine powder. FeSO₄ and FeCl₃ were obtained from Sigma-Aldrich (USA), while NaOH was purchased from Loba Chemi pvt ltd., India. All reagents and chemicals were used without further purification.

Synthesis of adsorbent: WM-Fe₃O₄

1.5: 1 of FeSO₄ to FeCl₃ were placed in a clean beaker followed by the addition of 100 mL of deionized water and 30 mL of 2.5 M NaOH. Mixing was carried out at 70 °C with constant stirring for 30 min. During this process, a black colouration was observed which indicated the formation of Fe₃O₄. 10 g of the watermelon rind powder was then added to the solution of magnetite under continuous stirring. The solution was then allowed to cool before filtration. This was then followed by washing and drying at 105 °C for 8 h. The synthesized material was thereafter stored in an air-tight container until use.

Characterization of WM-Fe₃O₄

The functional groups present on the prepared material were identified using FTIR [Shimadzu FT-IR 8400 s (class 1, Laser product)] and complemented with RAMAN spectroscopy; point of zero charge (pHpzc) was determined using the salt addition method (Simsek et al. 2016). The crystallinity of the prepared adsorbents was determined using XRD

recorded on a BRUKER AXS (Germany) X-ray Diffraction equipment from 0.5 to 130° 2θ at 0.5° s⁻¹; morphology was determined by SEM, while surface area was determined using Sear's method (Sear 1956).

Adsorption experiments

The adsorption behaviour of WM-Fe₃O₄ for Pb²⁺ was investigated in batch mode using 20 mg of the adsorbent with 10 mL aqueous solution of the metal ion. The pH of the solution was adjusted using 0.1 M NaOH or 0.1 M HCl. Samples were shaken at 150 rpm for 24 h, and the amount adsorbed q_e , was calculated using the equation below:

$$q_e = \frac{(C_o - C_e)}{m} V \quad (1)$$

where C_o and C_e are the initial and equilibrium concentrations of the metal ions in solution (mg/L), V is the volume of the solution (L) and m is the mass of the adsorbent (g).

The concentration of the metal ion remaining in solution was determined using Atomic Absorption Spectrophotometer (AAS). Each experiment was carried out in triplicates to determine the reproducibility of the results.

Equilibrium isotherm studies

20 mg of the adsorbents was added to 10 mL of Pb²⁺ solution with concentrations between 50 and 300 mg/L and agitated. The adsorption capacity, q_e (mg/g) after 24 h was determined using Eq. 1. The isotherms employed to describe the nature of the adsorption process are: Langmuir (L), Langmuir–Freundlich (L–F), Freundlich (F), Temkin (T) and Redlich–Peterson (R–P) isotherm models as outlined in Table 1.

Kinetic studies

Kinetic studies were carried out by agitating 10 mL of 100 mg/L Pb²⁺ with 20 mg of the adsorbent at different time intervals within 24 h and at room temperature. The adsorption capacity, q_t (mg/g) was estimated using Eq. 1. The experimental data obtained were analysed with four kinetic models: Pseudo first-order (PFOM), Pseudo second-order (PSOM), intraparticle diffusion (IPD) and Elovich kinetic models with their corresponding nonlinear equations outlined in Table 2.

All equilibrium and kinetic plots were made using KyPlot[®] software with the nonlinear mathematical versions of the equilibrium and kinetic models. KyPlot[®] uses the Quasi-Newton (least square) optimization tool for fitting the data to the models. The Normalized Standard Deviation (NSD) was used to determine the error value and by

Table 1 Adsorption isotherm model parameters for the adsorption of Pb²⁺ on WM-Fe₃O₄

Model	Equation	Parameter	
Freundlich	$q_e = K_F \cdot C_e^{1/n}$	K_F (L g ⁻¹)	19.69
		n	3.24
		R^2	0.621
		Error	892.90
Langmuir	$q_e = \frac{q_{max} \cdot K_L \cdot C_e}{1 + K_L \cdot C_e}$	q_{max} (mg/g)	138.19
		K_L (L mg ⁻¹)	0.015
		R_L	0.57
		R^2	0.724
		Error	691.89
Temkin	$q_e = \frac{RT}{b_T} \ln(K_T \cdot C_e)$	b_T (J mol ⁻¹)	32.78
		K_T (L mg ⁻¹)	0.118
		R^2	0.681
		Error	780.39
Langmuir–Freundlich	$q_e = \frac{Q^{\circ}(K_C C_e)^n}{1+(K_C C_e)^n}$	Q°	109.65
		K	0.017
		n	3.05
		R^2	0.835
		Error	661.34
Reedlich–Peterson		K_{RP}	1.02
		R_e	1.2×10^{-6}
		G	2.51
		R^2	0.938
		Error	261.95

Table 2 Kinetics model parameters for the adsorption of Pb²⁺ on WM-Fe₃O₄

Model	Equation	Parameter	
Pseudo first-order	$q_t = q_e - \exp(\ln q_e - K_1 t)$ (mg/g)	q_e (mg/g)	81.01
		K_1 (min ⁻¹)	0.84
		R^2	0.9023
		Error	9.87
Pseudo second-order	$q_t = \frac{q_e^2 K_2 t}{q_e K_2 t + 1}$	q_e (mg/g)	84.78
		K_2 (g/mg min)	0.023
		R^2	0.931
		Error	7.07
Elovich	$q_t = \frac{\ln \alpha \beta}{\beta} + \frac{1}{\beta} \ln t$	α (mg/g min)	0.158
		β (g/mg)	169.1
		R^2	0.915
		Error	8.68
Intraparticle diffusion	$q_t = K_{IPD} \cdot t^{1/2} + C$	K_{IPD}	0.023
		C	64.40
		R^2	0.884
		Error	11.63

extension, the model that best describes both kinetic and equilibrium data for the various adsorbents.

Results and discussion

Characterization of WM-Fe₃O₄

The FT-IR spectra of WM-Fe₃O₄ (Fig. 1) revealed the presence of Fe–O at 582 cm⁻¹ which shows the successful synthesis of magnetite. The highly intense and fairly broad band at 3401 cm⁻¹ revealed the presence of O–H stretching vibration present in the biomass. The band at 2925 cm⁻¹ corresponds to the presence of C–H bond characteristic of organic compounds. So is the band at 1238 cm⁻¹ which are attributed to phenolic and lactonic groups from the watermelon. The presence of bands at 1732 cm⁻¹ are characteristic of free and esterified carboxylic acid group which may be from pectin, while the band at 441 cm⁻¹ has been attributed to the presence of magnetic nanoparticles (Lasheen et al. 2016).

Surface area determination revealed the prepared composite to possess a surface area of 39 m²/g. Magnetite has been reported to impart high surface area in its composites (Ebrahimian et al. 2014; Wang et al. 2016). This is especially true considering that the surface area obtained in this study is greater than that obtained for untreated watermelon rind (15.1 m²/g) and treated watermelon rind (24 m²/g) (Memon et al. 2008).

Figure 2 shows the SEM image of WM-Fe₃O₄. The images show a compact rod-like structure with hexagonal pores at each end and the presence of numerous micropores which are most desired for adsorption. The pores showed different sizes attesting that WM-Fe₃O₄ is a heterogeneous composite with average pore size of 5 μm.

XRD pattern as shown in Fig. 3 indicates the presence of diffraction peaks at angles of 29.41°, 36.03°, 43.16°, 48.57°,

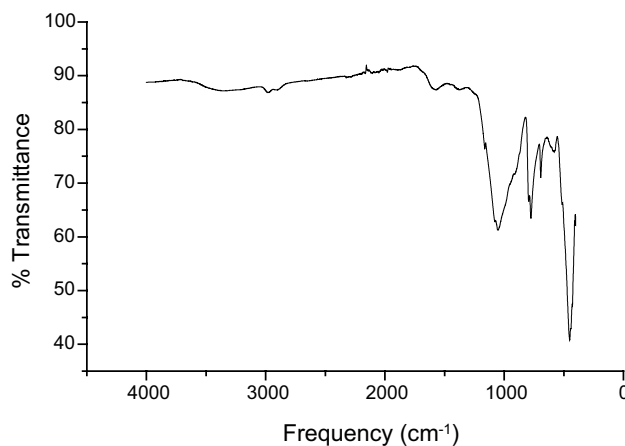


Fig. 1 FTIR spectrum of WM-Fe₃O₄

Fig. 2 SEM micrographs of WM-Fe₃O₄

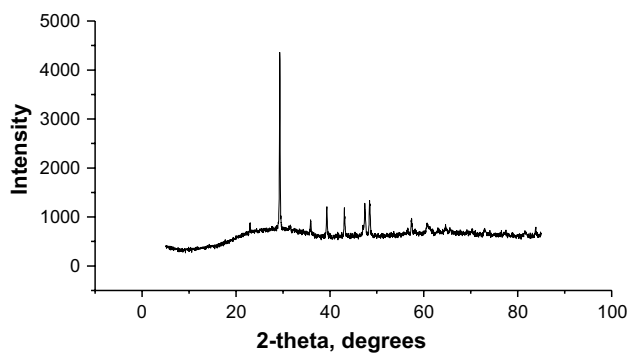
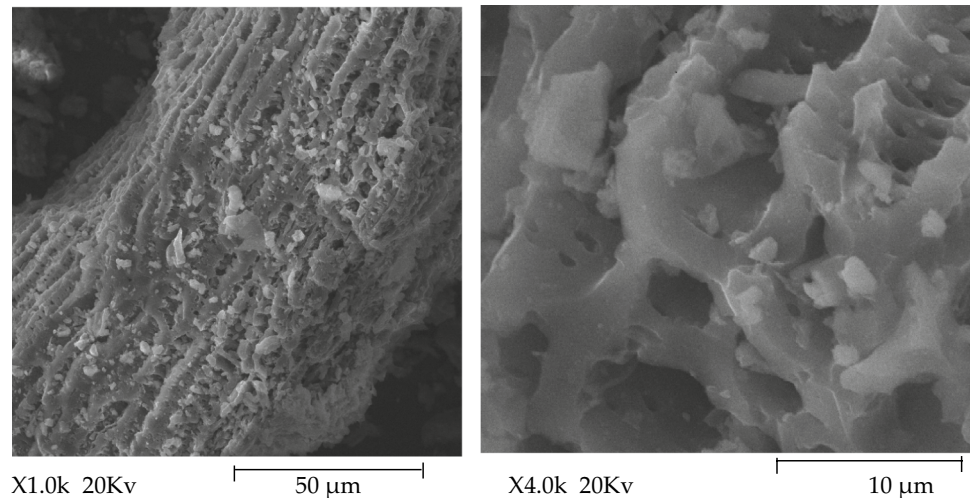


Fig. 3 XRD pattern for WM-Fe₃O₄

57.46° and 60.75° attesting to the presence of magnetite in the sample. They are assigned to crystal planes of 200, 311, 222, 400, 422 and 511, respectively. The XRD pattern illustrates the crystallinity and purity of WM-Fe₃O₄ as no diffraction peaks corresponding to ferrite nitrite or other iron oxides can be observed. Furthermore, the result obtained is in tandem with the result of FTIR confirming the formation of WM-Fe₃O₄. The crystalline size of WM-Fe₃O₄ was further estimated using the Debye–Scherrer equation (Yew et al. 2016):

$$d = \frac{k\lambda}{\beta_{hkl} \cos \theta_{hkl}}$$

where d is the crystalline size of synthesized material, k is the Scherrer's constant which is 0.9, λ is the X-ray wavelength of radiation for Cu-K α (0.154 nm), β_{hkl} is the full-width at half maximum in radian, and θ_{hkl} is the diffraction angle. Using the equation, the estimated crystalline size was found to be 2.83 nm.

The pH_{pzc}, which is the point at which the charge on the surface of the adsorbent is zero, was found to be 8.19.

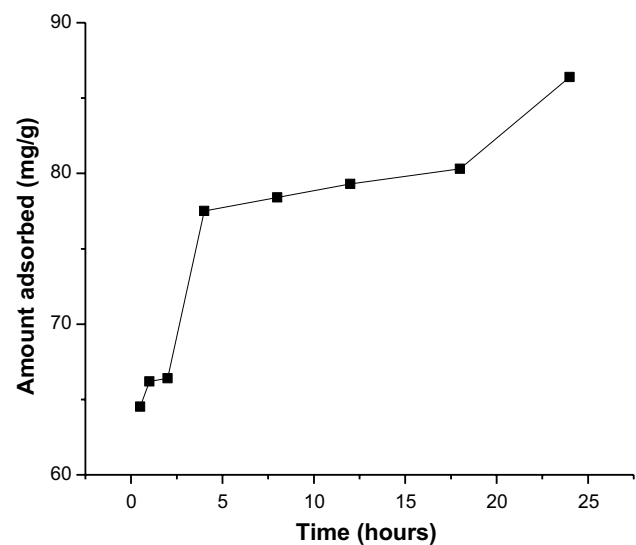


Fig. 4 Effect of contact time on adsorption of Pb²⁺ ions on WM-Fe₃O₄

Lakshmiopathy and Sarada (2016) have reported the pH_{pzc} of watermelon rind to be 4.9 (Banerjee et al. 2012). This shows that synthesizing a composite had an effect on the surface properties of WM-Fe₃O₄.

Adsorption studies

Effect of contact time

The effect of contact time was examined with increasing time from 30 min to 24 h (Fig. 4). This parameter is important because it helps in the design of the adsorption process. Also, it gives information on the rate of adsorption and helps in assessing the efficiency of the adsorbents in terms of maximizing operation time and increasing economic

benefits (Olu-Owolabi et al. 2012). As shown, there was an increase in the amount of Pb^{2+} adsorbed. Further increase in contact time beyond 2 h had negligible effect on the process (Shirzad-Shiboni et al. 2013). The further increase in adsorption beyond 12 h can be attributed to hydrolysis of lead ions which increased its apparent removal from solution. The point of maximum adsorption shows the point at which equilibrium was attained, and this is influenced by factors such as the nature of the adsorbent and adsorbate as well as the interactions between them (Fu et al. 2012). Increase in adsorption as contact time increases shows that up to the maximum point, all the active sites had not been fully covered by the ions. This coverage is affected by the rate at which the ions move through the bulk surface to the adsorbent and become attached to it. As the active sites fill with ions, this rate decreased hence the decrease in the rate of adsorption.

Effect of pH

pH is an important parameter because it influences the surface properties of the adsorbent as well as influence the interactions between the adsorbent and adsorbate (Dakhil 2013). Figure 5 shows that increasing the pH of the lead ion solution resulted in an initial decrease in adsorption. This can be attributed to the fact that at this low pH value, there is competition between the positive lead ions and H^+ for the active sites on the adsorbent. As the pH increases, this competition reduces and the uptake of lead ions increases. This is seen in the increase from pH 3 to 7. Beyond this optimal pH, there was no further decrease in adsorption. This trend could be due to the formation of soluble hydroxyl complexes of lead.

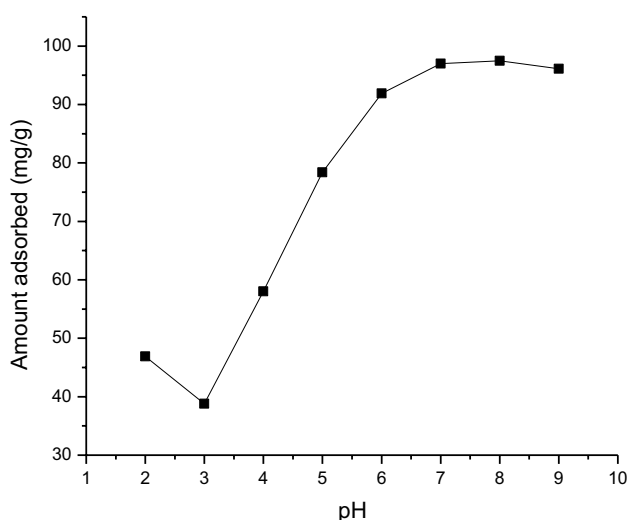


Fig. 5 Effect of pH on adsorption of Pb^{2+} ions on WM- Fe_3O_4

Effect of adsorbent dose

Studying the varying effect of adsorbent mass on adsorption efficiency is important in the optimization of dosage required the adsorption process thereby saving operation cost (Phatthanakittiphong and Seo 2016). Figure 6 shows the effect of varying adsorbent dosage on the adsorption of the lead ions in the range of 0.01–0.05 g. This variation resulted in an increase in adsorption up till 0.04 g for lead ions. This maximum value shows the point of saturation of the adsorbent for the metal ions. At lower dosage than this saturation point, increase in adsorbent mass resulted in an increase in number of active sites. This increased active sites led to increased adsorption up until the saturation maximum of 0.04 g. Further increase in mass however resulted in decrease in total surface area of the adsorbent and a reduction in the number of active sites available for adsorption as a result of aggregation of adsorbent particles. This aggregation becomes important as the mass of the adsorbent is increased (Abdus-Salam and Adekola 2018). This result also indicates that for efficient removal of these ions from solution, a low dosage of the adsorbent is required which favours its use on an industrial scale. Similar results were obtained by Zhang et al. (2018) with the adsorption of Cr(VI) ions on magnetic biochar. In their study, maximum adsorption was observed with 0.5 g/100 mL of the adsorbent beyond which no change in adsorption was found.

Effect of initial concentration

The effect of initial metal concentration on the adsorption of lead ions was studied with concentration increasing from 50 to 300 mg/L. From the plot in Fig. 7, it is observed

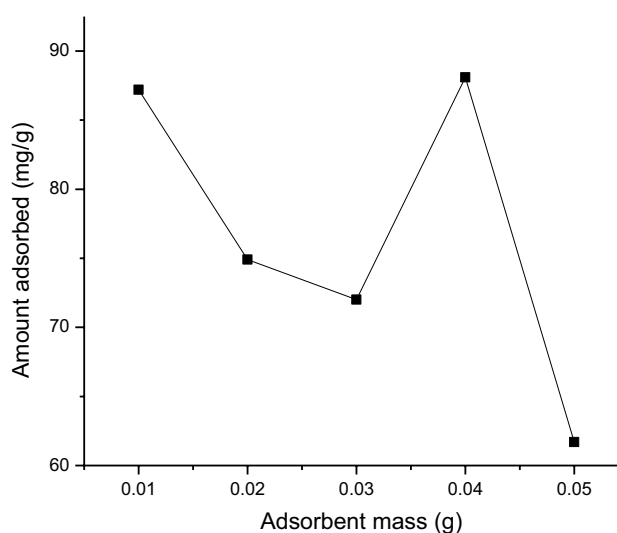


Fig. 6 Effect of adsorbent mass on adsorption of Pb^{2+} ions on WM- Fe_3O_4

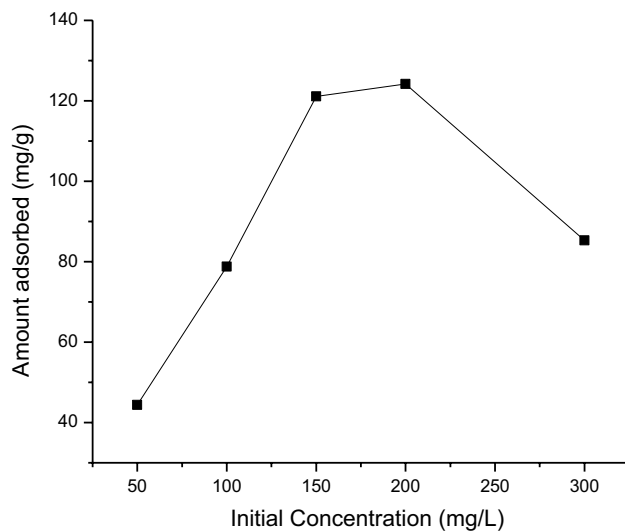


Fig. 7 Effect of initial pollutant concentration on adsorption of Pb^{2+} ions on $WM-Fe_3O_4$

that for the adsorption of lead ions, adsorption increased sharply from 50 to 150 mg/L. Decrease in amount adsorbed is observed from 200 mg/L. This shows that at low concentration, there were unoccupied active sites on the adsorbent which when filled by the ions resulted in increased adsorption coupled with increased mass transfer driving force of the ions to the adsorbent until the adsorbent became saturated and excess ions could not access any active sites. At this point, equilibrium is achieved and a further increase in the amount of the ions did not result in a further increase in adsorption.

Adsorption isotherms

Adsorption isotherms are essential for describing the mechanisms of interaction between adsorbents and adsorbates and speak to the feasibility of the adsorption process. The adsorption isotherm data were fitted to Langmuir, Freundlich, Temkin, Langmuir–Freundlich (L–F) and Redlich–Peterson (R–P) isotherm models using the nonlinear forms of their equations and their plots shown Fig. 8.

Of the five isotherms used in analysing the adsorption process, R–P isotherm, incorporates three parameters and combines the features of Langmuir, and Freundlich isotherms was the best fit for the adsorption of lead because it had the lowest error and highest R^2 value. R–P is used to predict the heterogeneous nature of the adsorption systems while circumventing the limitation of high adsorbate concentrations of Freundlich (Varank et al. 2012). This shows that both monolayer and multilayer are occurring simultaneously within the system, indicating that the adsorption could be driven by more than one force of attraction. L–F

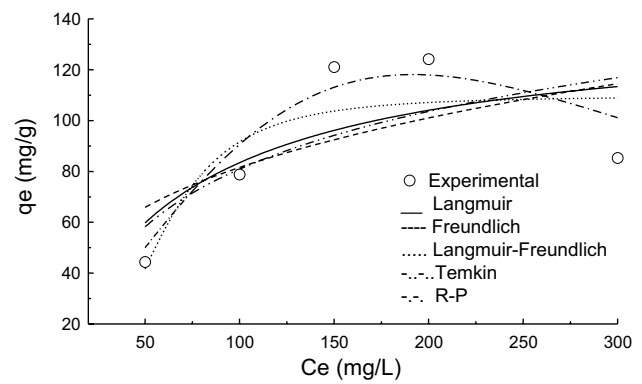


Fig. 8 Isotherm curves for the adsorption of Pb^{2+} ions on $WM-Fe_3O_4$ at 30 °C (initial pH: 6; adsorbent mass: 20 mg; contact time: 0–24 h)

isotherm follows closely in fitting the adsorption which further confirms that the adsorption involves a series of complex mechanisms (Zhu et al. 2015).

The maximum adsorption capacity given by the Langmuir isotherm which proposes that the surface of the adsorbent is uniform and adsorption occurs through the same mechanism is 138 mg/g as shown in Table 1. The value of Freundlich constant, n was greater than 1 indicating that the adsorption was favourable at studied conditions. This is corroborated by the n factor predicted using L–F model and further buttressed by the value of the dimensionless constants, R_L which was less than one. The surface heterogeneity of the adsorbent is attributed to the functional groups from the biomass and confirmed by FTIR.

Kinetic models

Modelling the experimental data to kinetic models is helpful in determining the uptake rate and equilibrium time. The data obtained in this study were modelled with four kinetic models: Pseudo first-order (PFOM), pseudo second-order (PSOM) kinetic model, Elovich and intraparticle diffusion (IPD) model. The best fit to the experimental data of lead adsorption was obtained for PSOM (Fig. 9) as it gave the highest R^2 values and lowest SE of all the models studied. A fit to PSOM shows that the adsorbent worked well over the whole range of adsorption time while implying chemical adsorption was involved (Samarghandi et al. 2009). The large rate constant (K_1) obtained (Table 2) shows how fast the reaction is. The value of K_1 was found to be greater than K_2 indicating that the adsorption is restricted by internal diffusion (Fang et al. 2017).

Intraparticle diffusion was used to analyse the predominant rate limiting step as well as quantify the effect of external mass transfer. If IPD is the rate limiting step, a plot of q_t versus $t^{0.5}$ should pass through the origin.

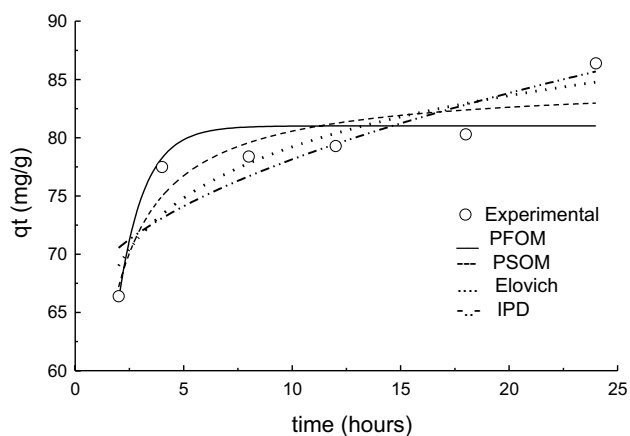


Fig. 9 Kinetics plots for the adsorption of Pb^{2+} ions on $\text{WM-Fe}_3\text{O}_4$ at $30\text{ }^\circ\text{C}$ (initial pH: 6; adsorbent mass: 20 mg; Initial Pb^{2+} concentration: 50–300 mg/L)

However, results obtained (Table 2) show that the mechanism of adsorption is perhaps complex as both internal diffusion and surface adsorption contribute to the adsorption. The high value of C obtained can be attributed to the high concentration at which the adsorption was studied as more chemical species competing for available sites increase the mass transfer.

Conclusion

This research studied the adsorption process of magnetite modified with watermelon rinds in the removal of lead ions from solution. The effect of varying experimental conditions such as pH, adsorbent dose, contact time and initial concentration were studied. pH was found to have a strong influence on the adsorption as increasing pH led to an increase in the amount adsorbed up to a maximum of 6. More than 70% of the adsorbates were removed in less than 5 min of contact showing that the adsorption was fast, an important consideration in scale up of polluted water treatment. Isotherm studies showed the adsorption to be favourable and feasible with a monolayer adsorption capacity of 138 mg/g. The predominant mechanism of interaction between the adsorbate and the adsorbent was found to be physical in nature. This is confirmed by the fact that the rate limiting step was not solely intraparticle diffusion. Hence, it can be said that the adsorbent possesses heterogeneous active sites which is responsible for the high adsorption capacity obtained. Therefore, $\text{WM-Fe}_3\text{O}_4$ is a highly efficient adsorbent that can be utilized on a large scale for the removal of heavy metals from wastewater.

Acknowledgements N/A.

Authors' contribution AOE contributed to the design and conception of the study, performed statistical analyses, interpreted the data and wrote the manuscript; KOA contributed to the design and conception of the study, interpretation of the data and critically revising the manuscript for important intellectual content while BTS performed the experiment that resulted in data used in the work. All authors reviewed the final draft of the manuscript and gave approval of the version to be published.

Funding N/A.

Compliance with ethical standards

Conflict of interest The authors declare that they have no conflict of interest.

Ethics approval Ethical approval not required as study did not involve human or animal subjects.

Availability of data and material The corresponding author, A. O. E may be contacted to request data.

Open Access This article is licensed under a Creative Commons Attribution 4.0 International License, which permits use, sharing, adaptation, distribution and reproduction in any medium or format, as long as you give appropriate credit to the original author(s) and the source, provide a link to the Creative Commons licence, and indicate if changes were made. The images or other third party material in this article are included in the article's Creative Commons licence, unless indicated otherwise in a credit line to the material. If material is not included in the article's Creative Commons licence and your intended use is not permitted by statutory regulation or exceeds the permitted use, you will need to obtain permission directly from the copyright holder. To view a copy of this licence, visit <http://creativecommons.org/licenses/by/4.0/>.

References

- Abdus-Salam N, Adekola SK (2018) Adsorption studies of zinc (II) on magnetite, baobab (*Adansonia digitata*) and magnetite-baobab composite. *Appl Water Sci* 8:222
- Adegoke HI, Amoo Adekola F, Fatoki OS, Ximba BJ (2014) Adsorption of Cr(VI) on synthetic hematite ($\alpha\text{-Fe}_2\text{O}_3$) nanoparticles of different morphologies. *Korean J Chem Eng* 31(1):142–154
- Banerjee K, Ramesh ST, Gandhimathi R, Nidheesh PV, Bharathi KS (2012) A novel agricultural waste adsorbent, watermelon for the removal of copper from aqueous solution. *Iran J Energy Environ* 3(2):143–156
- Dakhil I (2013) H: removal of phenol from industrial waste water using sawdust. *Res Inveny Int J Eng Sci* 3(1):25–31
- Ebrahimian AP, Saberikhah E, Kozani SSH (2014) Fe_3O_4 -wheat straw: preparation, characterization and its application for methylene blue adsorption. *Water Resour Ind* 7–8:23–37
- Fang Z, Hu Y, Wu X, Qin Y, Cheng J, Chen Y, Tan P, Li H (2017) A novel organic ascorbyl phosphate graphene-based monolith and its superior adsorption capability for bisphenol A. *Chem Eng J* 334:948–956
- Fisli A, Yusuf S, Syarofi R, Krisnandi YK, Gunlazuardi J (2014) Preparation and characterisation of magnetite-silica nanocomposite as adsorbent for removal of methylene blue dyes from environmental water samples. *Adv Mater Res* 896:525–531

- Fu D, Zhang Y, Lv F, Chu PK, Shang J (2012) Removal of organic materials from TNT red water by bamboo charcoal adsorption. *Chem Eng J* 193–194:39–49
- Hind A (2017) A: chemical composition, flavonoids and β -sitosterol contents of pulp and rind of watermelon fruit. *Pak J Nutr* 16(7):502–507
- Lakshmipathy R, Sarada NC (2016) Methylene blue adsorption onto native watermelon rind: batch and fixed bed column studies. *Desalination Water Treat* 57(23):1–14
- Lasheen MR, El-Sherif IY, Sabry DY, El-Wakeel ST, El-Shahat MF (2016) Adsorption of heavy metals from aqueous solution by magnetite nanoparticles and magnetite-kaolinite nanocomposite: equilibrium, isotherm and kinetic study. *Desalin Water Treat* 57(37):17421–17429
- Lodeiro C, Capelo JL, Oliveira E, Lodeiro JF (2019) New toxic emerging contaminants: beyond the toxicological effects. *Environ Sci Pollut Eff* 26:1–4
- Memon GZ, Bhangar MI, Akhtar M, Tapur FN, Memon JR (2008) Adsorption of methyl parathion pesticide from water using watermelon peels as a low cost adsorbent. *Chem Eng J* 18:616–621
- Olu-Owolabi BI, Oputu OU, Adebawale KO, Ogunolu O, Olujimi OO (2012) Biosorption of Cd^{2+} and Pb^{2+} ions onto mango stone and cocoa pod waste: kinetic and equilibrium studies. *Sci Res Essays* 7(15):1614–1629
- Phatthanakittiphong T, Seo GT (2016) Characteristic evaluation of graphene oxide for Bisphenol A in aqueous solution. *Nanomaterials* 6:128
- Pooi CK, Ng HY (2018) Review of low-cost point-of-use water treatment systems for developing communities. *NPJ Clean Water* 1:11
- Samarghandi MR, Hadi M, Moayedi S, Askari FB (2009) Two-parameter isotherms of methyl orange sorption by pinecone derived activated carbon. *Iran J Environ Health Sci Eng* 6(4):285–294
- Sear GW (1956) Determination of specific surface area of colloidal silica by titration with NaOH. *Anal Chem* 28(12):1981–1983
- Shirzad-Shiboni M, Jafari SJ, Farrokhi M, Yang JK (2013) Removal of phenol from aqueous solution by activated red mud: equilibrium and kinetic studies. *Environ Eng Resour* 18(4):247–252
- Simsek EB, Saloglu D, Ozcan W, Novak I, Berek D (2016) Carbon fibre embedded chitosan/PVA composites for decontamination of endocrine disrupting bisphenol A from water. *J Taiwan Inst Chem Eng* 70:291–301
- Toluwalase SOW, Owoeye R (2017) S: cost benefit analysis of watermelon production in Ekiti State, Nigeria. *RJOAS* 6(66):307–314
- Varank G, Demir A, Yetilmezsoy K, Top S, Sekman E, Bilgili MS (2012) Removal of 4-nitrophenol from aqueous solution by natural low cost adsorbents. *Indian J Chem Technol* 19:7–25
- Wang F, Yang B, Wang H, Song Q, Tan F, Cao Y (2016) Removal of ciprofloxacin from aqueous solution by a magnetic chitosan grafted graphene oxide composite. *J Mol Liq* 222:188–194
- Yew YP, Shameli K, Miyake M, Kuwano N, Khairudin NB, Mohamad SE, Lee KX (2016) Green synthesis of magnetite (Fe_3O_4) nanoparticles using seaweed (*Kappaphycus alvarezii*) extract. *Nanoscale Res Lett* 11:276–282
- Zhang X, Lv L, Qin Y, Xu M, Jia X, Chen Z (2018) Removal of aqueous Cr(VI) by a magnetic biochar derived from *Melia azedarach* wood. *Biores Technol* 250:1–10
- Zhu X, Tsang DCW, Chen F, Li S, Yang X (2015) Ciprofloxacin adsorption on graphene and granular activated carbon: kinetics, isotherms and effects of solution chemistry. *Environ Technol* 36(24):3084–3102

Publisher's Note Springer Nature remains neutral with regard to jurisdictional claims in published maps and institutional affiliations.